CANCER GENOMICS & PROTEOMICS *13*: 259-274 (2016)

Overexpression of HPV16 E6* Alters β-Integrin and Mitochondrial Dysfunction Pathways in Cervical Cancer Cells

WHITNEY EVANS[1,2], MARIA FILIPPOVA[1,2], VALERY FILIPPOV[1,2], SVETLANA BASHKIROVA[1,2], GUANGYU ZHANG[1,2], MARK E. REEVES[1,2,3] and PENELOPE DUERKSEN-HUGHES[1,2]

[1]Department of Basic Sciences and [2]Center for Health Disparities and Molecular Medicine, Loma Linda University School of Medicine, Loma Linda, CA, U.S.A.;
[3]Department of Surgery, Loma Linda University School of Medicine, and Surgical Oncology Research Laboratory, Loma Linda VA Medical Center, Loma Linda, CA, U.S.A.

Abstract. *Background: High-risk human papillomaviruses (HPV) cause nearly all cases of cervical cancer, as well as many types of oral and anogenital cancer. Alternative splicing increases the capacity of the HPV genome to encode the proteins necessary for successful completion of its infectious life cycle. However, the roles of these splice variants, including E6*, the smaller splice isoform of the E6 oncogene, in carcinogenesis are not clear. Materials and Methods: SiHa (HPV16$^+$) and C33A (HPV$^-$) cells were transfected with the E6* plasmid, and tandem mass tag-labeled protein levels were quantified by mass spectrometry. Proteomic analyses identified pathways affected by E6* in both HPV$^+$ and HPV$^-$ cells, and pathways were validated using in vitro methods. Results: A total of 4,300 proteins were identified and quantified in lysates of SiHa and C33A cells with and without HPV16 E6* expression. SiHa and C33A cells expressing E6* underwent changes in protein expression affecting integrin signaling and mitochondrial dysfunction pathways, respectively. Subsequent experiments were performed to validate selected E6*-mediated alterations in protein levels. Conclusion: E6* modifies the expression of proteins involved in mitochondrial dysfunction and oxidative phosphorylation in C33A cells, and β-integrin signaling in SiHa cells.*

Correspondence to: Penelope Duerksen-Hughes, Department of Basic Sciences, Loma Linda University School of Medicine, 11021 Campus Street, 101 Alumni Hall, Loma Linda, CA 92354. Tel: +1 9095584480, Fax: +1 9095584035, e-mail: pdhughes@llu.edu

Key Words: Human papillomavirus, E6*, alternative splicing, oxidative stress, RhoA GTPase, kindlin-1, alkaline phosphatase, cell spreading, DNA damage, mitochondrial membrane potential, oxidative phosphorylation, β-integrin, glutathione, mitochondrial membrane depolarization, electron transport chain, Ingenuity Pathway Analysis.

High-risk human papillomaviruses (HR-HPVs) cause cervical cancer in approximately 500,000 women annually, making it the third most common cancer in women worldwide (1, 2). Nearly half of these women will not survive. In addition to cervical cancer, HR-HPVs are the cause of malignancy in 60% of oropharyngeal cancer cases; 90% of anal cancer; 40% of vaginal, vulvar, and penile cancer; and cancer of other regions of the body such as the skin, colon, and rectum (3, 4). Numerous studies agree that the transformative properties of *E6* and *E7* are central to HPV-induced carcinogenesis, and the oncogenic roles of *E6* and *E7* have been well-characterized.

Increased cellular oxidative stress has been proposed to increase the likelihood that the virus will integrate into the host genome (5). This event often leads to up-regulation of *E6* and *E7* expression *via* disruption of the *E2* gene, causing increased cell survival and division through the weakening of pro-apoptotic processes and cell-cycle regulation, respectively. Although *E6* and *E7* are both considered indispensable for transformation efficiency, *E6* can, in some instances, immortalize cells in the absence of *E7*, indicating that *E6*-dependent mechanisms underlying cervical carcinogenesis are of vital importance (6-8).

Interestingly, high- but not low-risk HPVs generate multiple transcripts of full-length *E6* mRNA *via* alternative splicing (9, 10). In mammalian cells, the HR-HPV E6 oncoprotein is expressed as both full-length and spliced isoforms, with the smaller isoforms (generally referred to as E6*) corresponding approximately to the *N*-terminal third of the full-length protein. Relatively little is known about the smaller variants as compared to the full-length isoform, and *E6* splicing patterns vary between HR-HPV types (11-13). Alternative splicing enables the virus to expand its proteome from a modestly-sized genome, thereby increasing the genetic diversity and persistence of the virus against host immunity and raising its chance of survival (14).

Previously, our group demonstrated that the overexpression of E6* reduced tumor growth by both HPV^+ SiHa and HPV^- C33A cervical carcinoma cells in a nude mouse xenograft model (13), raising the question of what changes in cellular pathway activation might contribute to the E6*-mediated decrease in tumor size. In the present study, proteomic analyses of HPV^+ (SiHa) and HPV^- (C33A) cervical carcinoma cells were used to demonstrate how E6* influences protein expression, and to examine the impact such modifications have on the activation of cellular pathways *in vitro*. Additionally, we sought insight into how E6* may affect tumor growth through its effects on these pathways.

Materials and Methods

Reagents. Monoclonal antibodies against kindlin-1 and polyclonal β-1 integrin were obtained from Millipore Chemicon (Temecula, CA, USA), while those to RAS homolog gene family, member A (RHOA) and glyceraldehyde 3-phosphate dehydrogenase (GAPDH) were acquired from Cell Signal Technology (Beverly, MA, USA). α-Flag agarose, α-Flag-HRP antibodies, MG132, a reversible proteasome inhibitor, and α-β-actin were purchased from Sigma-Aldrich (St. Louis, MO, USA). Secondary fluorescent antibodies were obtained from LI-COR Biosciences (Lincoln, NE, USA).

Cell culture. SiHa and C33A cells, derived from human cervical carcinomas, were obtained from the American Type Culture Collection (Manassas, VA, USA). All cells were cultured in modified Eagle's medium (MEM) (Thermo Fisher Scientific, Hanover Park, IL, USA) and supplemented with 10% fetal bovine serum (Invitrogen, Carlsbad, CA, USA), penicillin (100 μg/ml), and streptomycin (100 μg/ml) (Sigma-Aldrich, St. Louis, MO, USA).

Plasmids, transfection, and the creation of stable cell lines. The pFlag-E6* (pE6*) plasmid was constructed by cloning *E6*I* in frame with the *N*-terminal Flag-tag and the C-terminal C-myc-tag into the pFlag-Myc CMV-22 vector (Sigma-Aldrich). Stable cell lines expressing pE6* or vector control (*e.g.* pFlag) were produced using the Mirus Bio transfection kit, TransIt-LT1 Transfection reagent (Thermo Fisher Scientific), to transfect the appropriate plasmids into SiHa and C33A cells, as directed by the manufacturer. G418 (neomycin, which is an aminoglycoside antibiotic) (500-800 μg/ml) was added to cells 48 h post-transfection and antibiotic selection was carried out for 3 weeks. Subsequently, expression of E6* was evaluated by immunoblot analysis.

Immunoblot analysis. Approximately 10^6 cells were lysed in ~100 μl lysis buffer, and lysates were sonicated and separated by sodium dodecyl sulfate polyacrylamide gel electrophoresis followed by protein transfer onto polyvinylidene difluoride membranes (Thermo Fisher Scientific). Membranes were blocked with 1% bovine serum albumin, and primary antibodies (α-mouse or α-rabbit) in Tris-buffered saline and Tween 20 (TBST) were applied overnight at 4˚C. Membranes were washed with TBST the following day. Secondary Immunopure Antibodies (α-mouse or α-rabbit) conjugated to horseradish peroxidase (Thermo Fisher Scientific) were incubated with the membrane for 1 h. Chemiluminescent SuperSignal West Dura and Pico Maximum Sensitivity substrates were used to detect signals. In the case of fluorescent secondary antibodies (LI-COR, Lincoln, NE, USA), signals were detected using the Odyssey imaging system and relative densities were quantified against standard controls using ImageJ software analysis [v1.48; see reference (15)].

Microscopy. Morphological analysis of SiHa and C33A cells was conducted using an Olympus IX70 inverted microscope (Olympus America, Center Valley, PA, USA). Cells were seeded at a density of 10^3 per 100×20 mm tissue culture-treated dish 3-7 days prior to imaging. Live images, using Hoffman Modulation contrast, were captured with a digital SPOT RT3™ camera and SPOT Insight software (SPOT Imaging, Sterling Heights, MI, USA). All images were acquired with uniform settings and magnification (×20).

Mitochondrial membrane depolarization. The Mito-ID membrane potential detection kit (Enzo Life Sciences, Farmingdale, NY, USA) was used as directed by the manufacturer. Mitochondrial membrane depolarization was estimated using the dual-emission mitochondrial membrane potential (MMP)-sensitive dye, cationic carbocyanine. Following treatment, cells were collected in 1X phosphate buffered saline and analyzed on a Becton-Dickinson FACSCalibur FLOW cytometer (Becton-Dickinson, San Francisco, CA, USA). The FL-1 channel detected depolarized mitochondria, indicated by green fluorescence, while the FL-2 channel gathered orange fluorescence from energized mitochondria. The data were collected and analyzed using Flow-Jo software (Ashland, OR, USA).

Secreted embryonic alkaline phosphatase analysis. Alkaline phosphatase activity was measured using the Great EscAPe SEAP Detection Kit provided by BD Biosciences (Clontech, Mountain View, CA, USA) as directed by the manufacturer. Lysates of SiHa and C33A cells were collected and a luminometer was used to detect signals produced by the phosphatase/substrate reaction. This measured activity was normalized against total protein concentration, which was acquired by a spectrophotometer plate reader.

Proteomic analysis. Protein lysates were collected from ~5×10^6 cells from each of the cell lines (SiHa pFlag, SiHa E6*, C33A pFlag, and C33A E6*). Samples were sonicated, denatured, reduced, and alkylated as recommended by the directions provided with the TMT Mass Tagging Kit (Thermo Fisher Scientific,). Cell lysates were prepared, run on an LTQ-Orbitrap Velos mass spectrometer (Thermo Fisher Scientific) and analyzed as previously described (16). Protein identification from each mass spectrometry raw data file was performed against the human library using Proteome Discoverer 1.2 software (Thermo Fisher) with a signal to noise threshold of 1.5. A false-discovery rate of less than 1% was applied and detection included that of unique peptides only. A fold change cut-off value of 1.5, comparing one group of cells (*e.g.* E6* overexpressing cells) to a control group of cells, (*e.g.* pFlag vector-containing cells) was applied during Ingenuity Pathway Analyses.

Comet assay. To measure nuclear DNA damage in SiHa and C33A cells, the Comet assay kit was obtained from Trevigen (Trevigen, Gaithersburg, MD, USA) and used according to the manufacturer's instructions as previously described (17). Briefly, cells were lysed and gel electrophoresis was carried out under alkaline conditions. SYBR gold from Invitrogen was used to stain cells. One hundred DNA tails were photographed and analyzed on a BIOREVO fluorescence microscope (BZ-9000) (Keyence Corporation, Itasca,

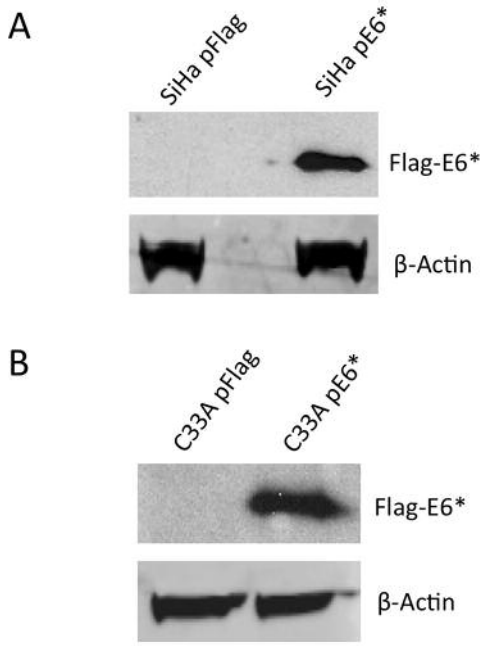

Figure 1. *Expression of E6*I (E6*) in HPV⁺ SiHa (A) and HPV⁻ C33A (B) cells. Cells were stably transfected with Flag-E6*I or empty pFlag vector, and E6*-expressing clones were selected by resistance to G418. E6* expression of cells in pooled clones was analyzed by immunoprecipitation with α-Flag agarose, followed by detection using antibodies directed against Flag-Horseradish peroxidase. α-β-Actin antibodies were used to normalize for immunoprecipitation input.*

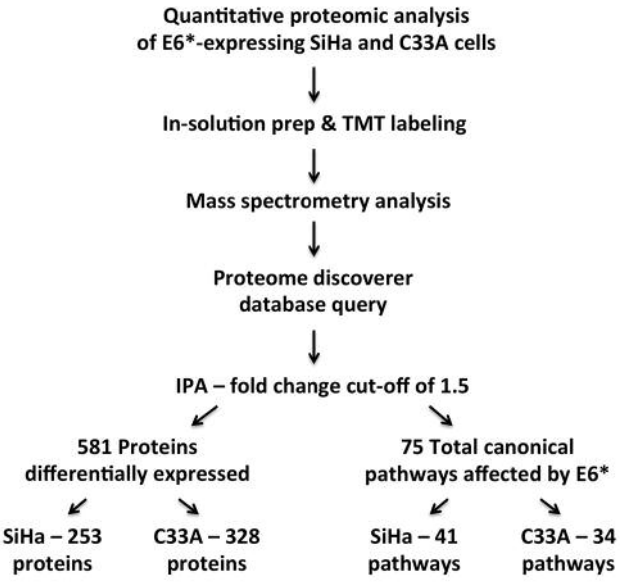

Figure 2. *Workflow for the relative quantitative analysis of SiHa and C33A cell lysates by mass spectrometry and Ingenuity Pathway Analysis. Proteins from cell lysates were reduced and alkylated for subsequent trypsinization, and the resulting peptides were labeled using multi-plex tandem mass tags (TMT) for quantitation of proteins from each sample. Labeled peptides were combined and fractionated using strong cation exchange in increasing concentrations of KCl solution. Sample enrichment was performed using Pierce C18 tips. Identical proteins from the different samples were separated and quantified according to isobaric tag labeling. Proteins identified by mass spectrometry were compared against the Proteome Discoverer human library. Raw Data files were uploaded to IPA and a fold-change of 1.5 was applied to filter insignificant changes in protein levels between cells expressing E6* and those not expressing E6*. Core analysis revealed that the levels of 581 proteins from SiHa and C33A cells were affected by E6* expression and that 75 pathways were involved in these cellular proteomic changes.*

IL, USA) with Comet IV software (Perceptive Instruments Ltd., St Frances House, Bury St Edmunds, UK) using uniform magnification (×10 for counting; ×20 for photographs) and settings.

Glutathione (GSH) assay. The GSH-Glo assay from Promega (Madison, Wisconsin) was used to quantify glutathione levels in SiHa and C33A cells. Cell lysates were placed in 96-well plates and GSH levels were detected by luminescence following a coupled reaction between firefly luciferase and GSH-S-transferase. Background luminescence was subtracted from that for GSH for each sample and the values were converted to molar GSH concentrations based on a standard curve. Total protein concentration was measured using a spectrophotometer plate reader. The average GSH concentration from each sample well was divided by the same well's corresponding total protein concentration to yield the reported ratio (μM/mg).

Statistics. All experiments were repeated at least three times with results reported as mean±standard deviation. Student's *t*-test was used to analyze differences, and a *p*-value of less than 0.05 was considered significant.

Results

E6 expression alters pathway activation in both HPV⁺ and HPV⁻ contexts.* Our first task in determining how E6* affects the cellular proteome was to overexpress E6* in both HPV⁺ and HPV⁻ systems. Therefore, HPV⁺ SiHa and HPV⁻ C33A cervical cancer cells were stably transfected with either the empty vector pFlag, or with pE6* to create clones with either very low/lack of (SiHa pFlag and C33A pFlag, respectively) or high (SiHa pE6* and C33A pE6*, respectively) E6* expression. Following selection of the E6* cells using G418, equal numbers of cells from the three clones with the highest levels of E6* expression were combined (SiHa pE6*; C33A pE6*) (Figure 1A and B, respectively).

To determine the effect of HPV16 E6* on the levels of cellular proteins, and to thereby gain insight into how this small viral protein orchestrates cellular activities in the presence and absence of full-length E6, protein expression in SiHa pFlag, SiHa pE6*, C33A pFlag and C33A pE6* cells was evaluated using mass spectrometry followed by pathway analysis as indicated by the scheme shown in Figure 2. Data were analyzed through the use of QIAGEN's Ingenuity Pathway Analysis (IPA), (Redwood City, www.qiagen.com/ingenuity).

Mass spectroscopy identified a total of 4,300 proteins. Based on a 1.5-fold change as the cut-off value, 253 proteins for SiHa cells and 328 proteins for C33A cells were selected for further IPA investigation. Together, the analyses for SiHa and C33A cells revealed a total of 75 pathways whose proteins exhibited statistically significant changes in expression (using a fold change cut-off value of 1.30=negative log of 0.05 as the *p*-value) in the presence of *E6**. The top 10 cellular pathways affected by E6* for SiHa and C33A cells are presented in Tables I and II, respectively. IPA revealed that integrin-linked kinase (ILK) signaling was the pathway most altered by E6* overexpression in SiHa cells, while oxidative phosphorylation (OXPHOS) and mitochondrial dysfunction pathways were influenced the most in C33A pE6* cells.

E6 expression in SiHa cells affects the β-integrin pathway and cell morphology.* IPA analysis suggested involvement of β-integrin signaling, *via* ILK, in response to E6* overexpression in SiHa cells (Figure 3A). ILK is known to bind the cytoplasmic domain of β1-integrin (18). To verify the biological effect of *E6** on β-integrin pathways in SiHa cells, immunoblot and phase-contrast microscopy analyses were conducted. Immunoblot data suggest that overexpression of E6* in SiHa cells increased cellular levels of β1-integrin (Figure 3B), a finding consistent with the proteomic data. To confirm activation of β1-integrin, we probed for the expression of kindlin-1, a co-stimulatory molecule of β1-integrin. We found that kindlin-1 expression in SiHa pE6* cells was significantly ($p<0.05$) increased (Figure 3C), reinforcing the notion that E6* stimulates the β-integrin signal cascade in SiHa cells, but not in C33A cells, consistent with the mass spectroscopic analysis.

Notably, kindlin-1 regulates cytoskeleton components by targeting Rho family GTPases (19). Therefore, *E6**-expressing SiHa and C33A cells were evaluated for RhoA GTPase (RhoA) expression to further investigate the possible downstream effects of β-integrin signaling. Figure 3D shows that SiHa E6* cells express reduced levels of RhoA as compared to SiHa pFlag cells ($p<0.05$). C33A pE6* cells also exhibited a slight decrease in RhoA levels compared to C33A pFlag cells, although statistical significance was not achieved. Interestingly, RhoA is implicated in cell motility (20) and cytoskeletal reorganization (21), suggesting that E6* might operate through kindlin-mediated RhoA expression to regulate cell shape (22) in SiHa cells.

To test whether *E6** causes changes in morphology of cervical cancer cells with active β-integrin signaling, we analyzed SiHa and C33A cells by microscopic imaging using Hoffman Modulation contrast, which showed conspicuous morphological changes resembling cell spreading and outward membrane protrusion of SiHa E6* cells as compared to SiHa pFlag cells (Figure 4A), although these changes were not seen in C33A cells (Figure 4B). Collectively, the data presented here suggest that E6* may directly or indirectly affect key components of the integrin signaling pathway in SiHa, but not C33A cells.

Table I. *Top 10 canonical pathways affected by E6* overexpression in SiHa cells. Ingenuity Pathway Analysis revealed that E6* expression in SiHa cells significantly influences multiple pathways including the Integrin-linked kinase (ILK) pathway.*

Ingenuity Canonical Pathways - SiHa E6*/SiHa pFlag	*p*-Value
ILK signaling	9.77×10^{-7}
Role of BRCA1 in DNA damage response	8.51×10^{-6}
Virus entry via endocytic pathways	2.29×10^{-5}
Caveolar-mediated endocytosis signaling	4.46×10^{-5}
Agranulocyte adhesion and diapedesis	1.07×10^{-4}
Clathrin-mediated endocytosis signaling	1.70×10^{-4}
Hereditary breast cancer signaling	2.75×10^{-4}
Purine nucleotides *de novo* biosynthesis II	3.55×10^{-4}
5-aminoimidazole ribonucleotide biosynthesis 1	5.25×10^{-4}
AMPK signaling	7.41×10^{-4}

*AMPK: AMP-activated protein kinase; *BRCA: breast cancer gene 1.

Table II. *Top 10 canonical pathways affected by E6* expression in C33A cells. Overexpression of E6* in C33A resulted in significant changes to several pathways, including the oxidative phosphorylation (OXPHOS) and mitochondrial dysfunction pathways.*

Ingenuity Canonical pathways - C33A E6*/C33A pFlag	*p*-Value
Oxidative phosphorylation	1.26×10^{-19}
Mitochondrial dysfunction	3.16×10^{-19}
TCA cycle II (eukaryotic)	6.61×10^{-8}
Proline biosynthesis 1	7.59×10^{-8}
2-ketoglutarate dehydrogenase complex	1.82×1^{-5}
Proline biosynthesis II (from arginine)	8.91×10^{-5}
Arginine degradation VI (arginase 2 pathway)	8.91×10^{-5}
Granzyme A signaling	1.51×10^{-4}
Valine degradation 1	1.95×10^{-4}

Alkaline phosphatase (ALPP) activity is significantly reduced in SiHa, but not in C33A cells following E6 overexpression.* In addition to the β-integrin pathway analysis, several individual SiHa cellular proteins affected by the overexpression of E6* were noted; placental ALPP was one of these proteins. ALPP was of particular interest because this was one of the proteins with the highest fold-change; moreover, high ALPP is correlated with pluripotency and undifferentiated cell phenotypes, while low ALPP implies differentiation (23). Furthermore, the tumors of patients with decreased ALPP levels tend to progress more slowly than those with higher ALPP levels (24, 25). The secreted

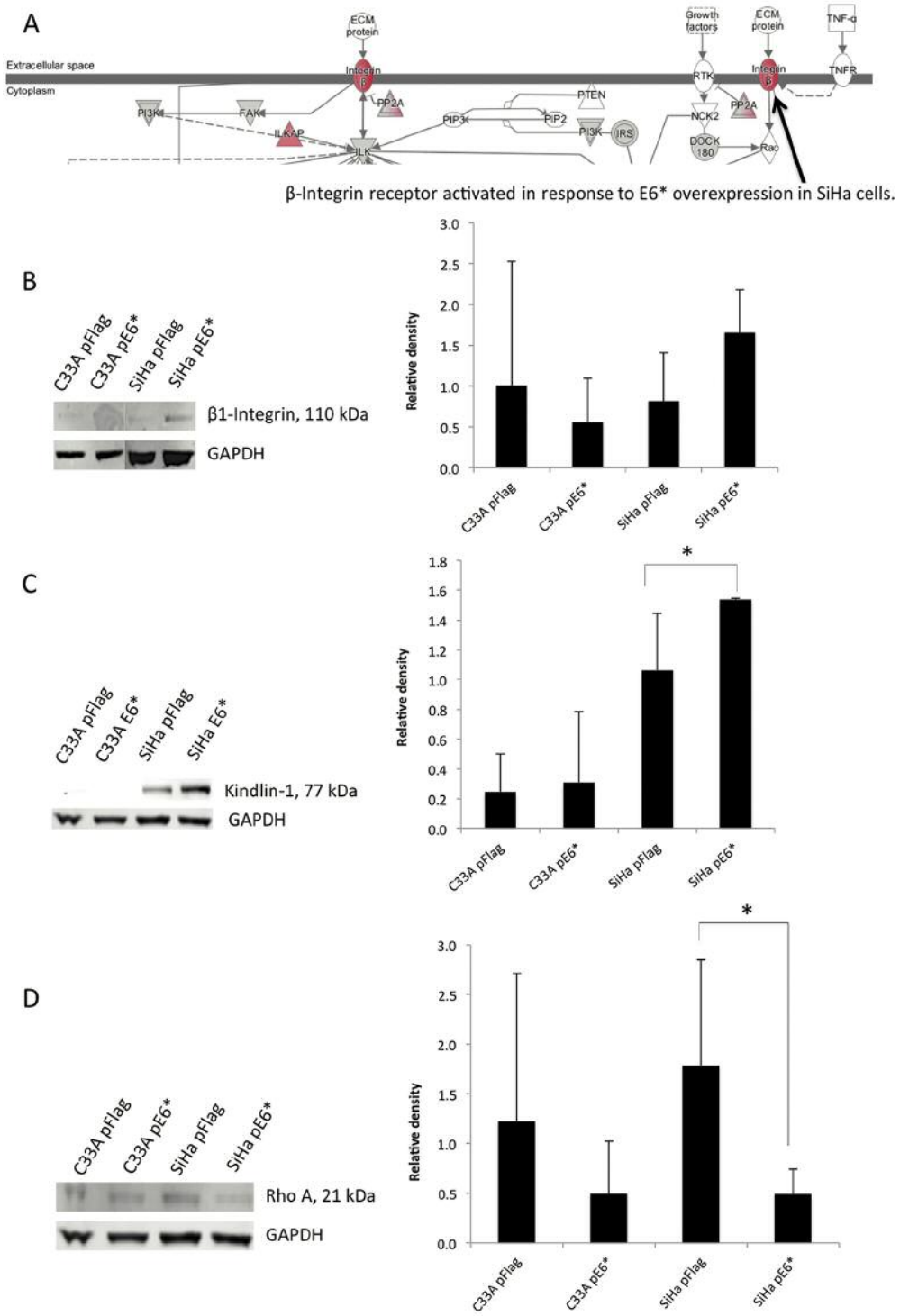

Figure 3. *Activation of β-integrin signaling by overexpression of E6* in SiHa cells. A: Increased expression of several members of the β-integrin signaling pathway in SiHa cells overexpressing E6* (pE6*) compared to SiHa pFlag cells; red color tones suggest an up-regulation of molecules compared to control cells. B: Immunoblot of SiHa cells showed increased expression of β1-integrin in cells overexpressing E6* compared to controls. C33A cells expressing and not expressing E6* displayed no discernible difference in β1-integrin levels. C: Increased expression of an upstream regulator of β-integrin signaling, kindlin-1, was detected in SiHa pE6* cells compared to SiHa pFlag cells. C33A cells exhibited no measurable difference in kindlin-1 expression. D: A decrease in Ras homolog gene family, member A (RhoA) expression, which is downstream of β1-integrin and kindlin-1 regulation, was also detected in SiHa pE6* cells, with the same trend observed in C33A pE6* cells. The relative density of three repeats is presented in the graphs, and error bars represent the standard deviations. *Significantly different at $p<0.05$.*

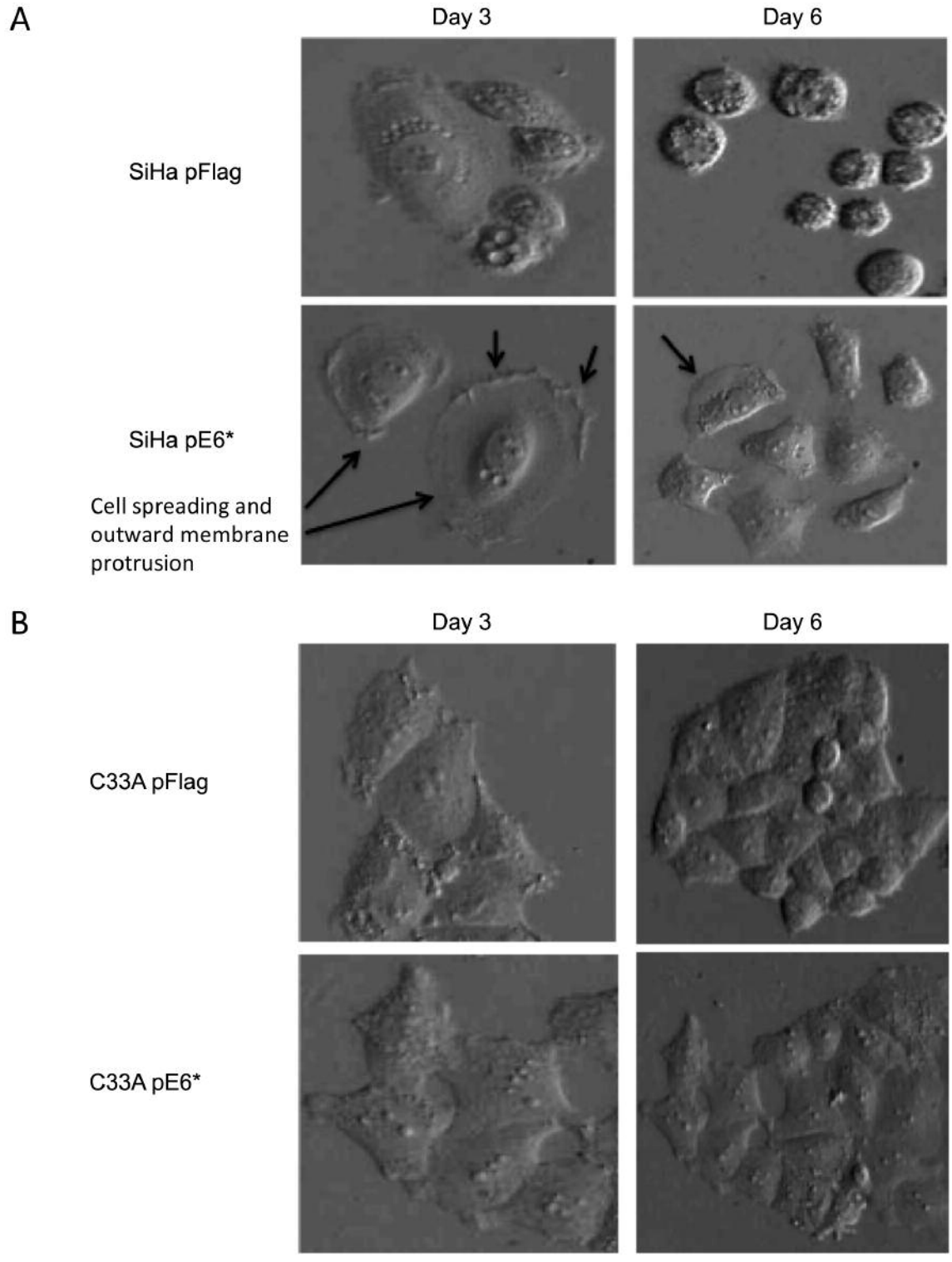

Figure 4. *Morphological analysis of SiHa pFlag and SiHa pE6* cells by microscopy. A: Images of SiHa cells captured using Hoffman modulation contrast (×20) show differences in cell appearance between cells overexpressing E6* and those transfected with the empty vector. Top panels show SiHa pFlag cells approximately 3-6 days following seeding at a cell density of 10^3 while the bottom panels show images of SiHa pE6* cells acquired at the same time. SiHa pE6* cells can be described as exhibiting more cell spreading and membrane protrusion (black arrows) as compared to the more closely positioned SiHa pFlag cells. B: Images of C33A pFlag and C33A pE6* cell obtained under the same conditions (Hoffman modulation contrast at 3-7 days; (×20) as SiHa cells did not demonstrate cell spreading behavior.*

embryonic AP assay was utilized to investigate the effect of E6* on ALPP activity in SiHa cells, since embryonic AP is a truncated form of ALPP. Our data demonstrate that *E6** reduces the activity of ALPP in HPV^+ SiHa cervical cancer cells ($p<0.05$; Figure 5), which is consistent with a predicted association between lower serum ALPP levels and better clinical outcomes in certain cancers (26). However, ALPP activity was not greatly affected in HPV^- C33A cervical cancer cells expressing E6*.

E6 impairs mitochondrial function in SiHa pE6* cells and affects the mitochondrial dysfunction pathway in C33A cells.* Proteomic analysis revealed that expression of E6* in C33A cells interferes with the overlapping mitochondrial dysfunction and OXPHOS pathways. Figures 6A and B illustrate that the proteins most perturbed due to *E6** expression in C33A cells are involved in the electron transport chain (27), located in the inner mitochondrial membrane, and that these proteins play roles in both the mitochondrial dysfunction and OXPHOS pathways. Since mitochondrial function is linked to the maintenance of mitochondrial membrane depolarization (MMP) (28), we measured MMP in SiHa and C33A cells by the Mito ID assay and flow cytometry.

Mito ID analysis demonstrated a modest increase in mitochondrial membrane depolarization in C33A pE6* cells compared to C33A control cells. Mitochondrial membrane depolarization was detected by the FL-1 channel and is indicated by the migration of carbocyanine dye out of the organelle (Figure 7A, left bars and histogram). Additionally, our data suggest an increase in energized mitochondria in C33A pE6* cells compared to controls, as shown by the FL-2 channel (Figure 7A, right bars and histogram). The FL-2 channel detects orange fluorescence caused by dye aggregation in mitochondria with an intact membrane potential, therefore implying an increase in energized mitochondria. Surprisingly, although proteomic analysis did not detect changes in the expression of proteins involved in mitochondrial dysfunction in SiHa pE6* cells as compared to SiHa controls, Mito ID analysis of the MMP in SiHa cells demonstrated that mitochondrial membrane depolarization was modestly more pronounced in SiHa pE6* cells compared to SiHa pFlag cells (Figures 7B, left bars and histogram). This finding is indicated by an increase in membrane permeability and a reduction in dye aggregation in the organelle (FL-1 channel). Furthermore, SiHa pE6* cells exhibited decreased orange fluorescence (FL-2 channel, right bars and histogram), implying a less energized population of mitochondria compared to SiHa pFlag cells.

Increased DNA damage in C33A E6 and SiHa E6* cells accompanies a reduction in GSH level.* Increased reactive oxygen species (ROS) due to mitochondrial dysfunction causes cellular oxidative stress and DNA damage (17, 29).

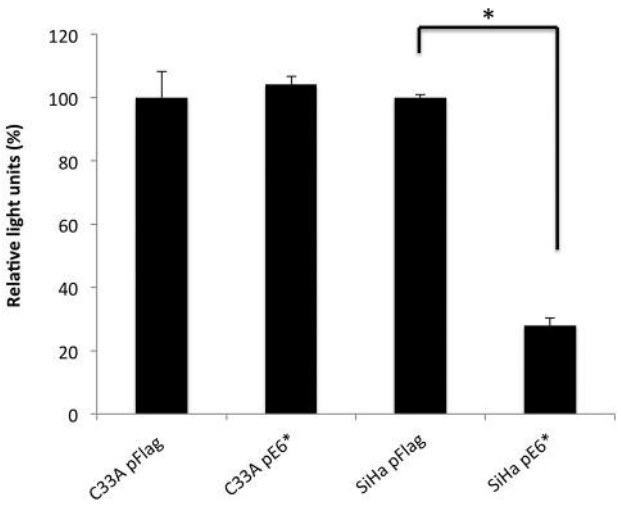

Figure 5. *E6* overexpression reduces alkaline phosphatase (AP) levels in SiHa but not C33A cells. Cell lysates were collected to measure AP levels in triplicate, and the Great EscAPe SEAP Detection Kit by BD Biosciences was used to detect E6*-mediated changes in AP expression in cells. When AP was normalized against protein concentration, we found that AP levels in SiHa pE6* cells were greatly reduced compared to SiHa pFlag cells. No decrease in AP was detected in C33A cells. The relative light units of triplicate measurements are presented in the graphs, and error bars represent the standard deviations. *Significantly different at p<0.05.*

Therefore, markers of oxidative stress, such as a decrease in expression of antioxidant enzymes, or the presence of DNA damage, can be harbingers of a cell population's inability to manage oxidative stress that surpasses the tolerance threshold. We, therefore, employed the comet assay to measure DNA damage and assessed GSH levels to estimate antioxidant defense in E6*-expressing SiHa and C33A cells.

Figure 8A shows representative images from the comet assays performed on SiHa and C33A cells transfected with pFlag or pE6*. We found that SiHa and C33A pFlag cells had approximately the same amount of DNA damage and an equivalent distribution of cells with minimal to medium migration patterns (scores of 50-100 or 100-150, respectively) (Figure 8B). However, when the *E6**-expressing cells were compared with each other and to their pFlag controls, different trends emerge. SiHa pE6* cells displayed the most severe DNA damage among the four lines tested, with greater than ~60% of the cell population displaying medium DNA damage (score of 100-150), and the remaining 40% divided between undamaged and minimal damage (scores of 0-50 or 50-100, respectively). In contrast, the DNA damage observed in SiHa pFlag cells was divided evenly into thirds between the varying levels of comet tail lengths. Surprisingly, C33A pE6* cells displayed slightly less medium DNA damage than did the C33A

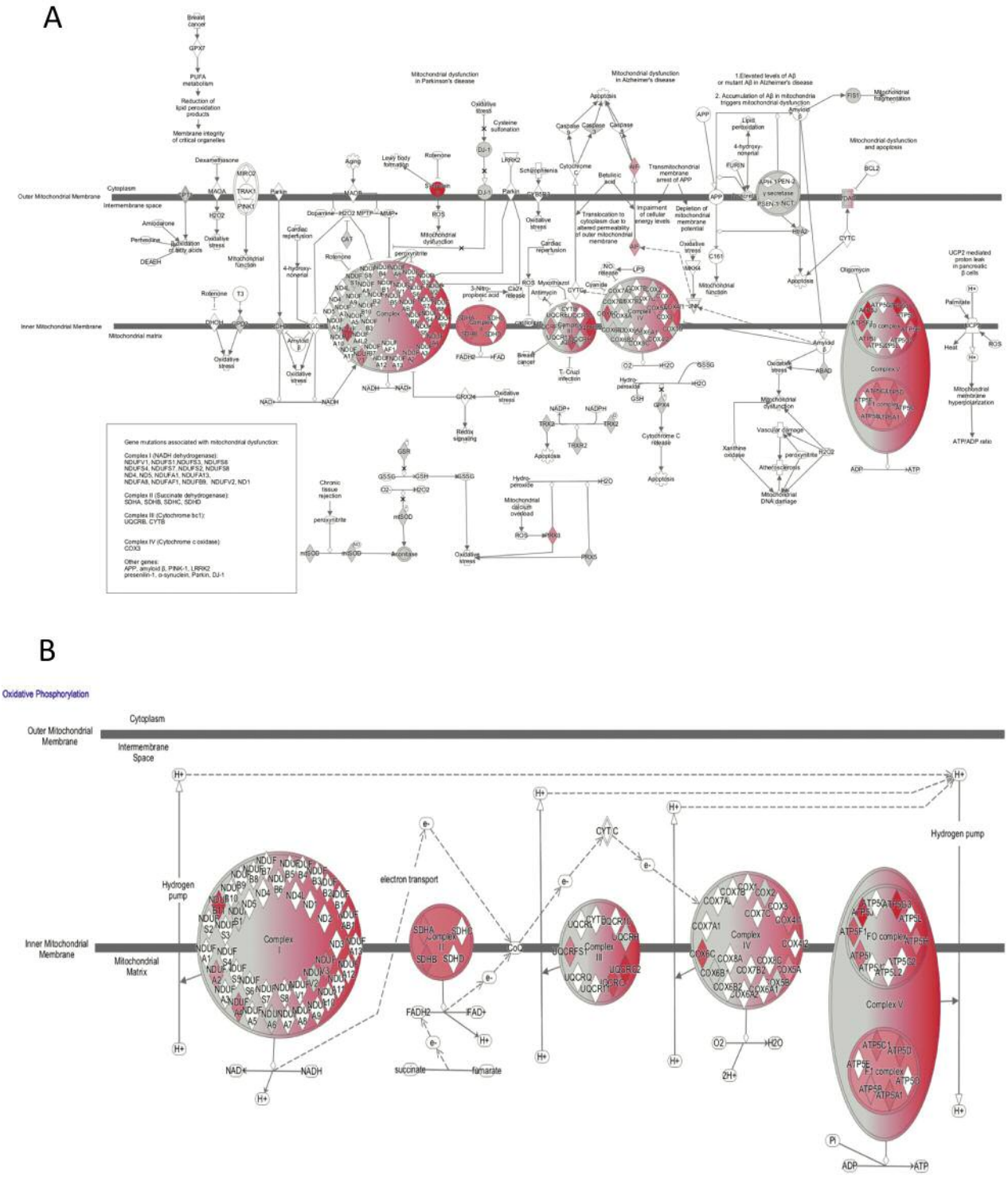

Figure 6. *Expression of E6* in C33A cells affects mitochondria. A: Pathway analysis comparing over-/underexpression of proteins in C33A pE6* cells compared to C33A pFlag cells indicates considerable involvement of the mitochondrial dysfunction pathway in E6*-expressing C33A cells. Molecules affected by E6* in C33A pE6* cells include those associated with the protein complexes of the electron transport chain within mitochondria, with the red color tones denoting increased expression in C33A pE6* cells. B: The oxidative phosphorylation canonical pathway, which is closely related to the mitochondrial dysfunction pathway, also experienced changes in protein expression due to E6* expression in C33A cells. Consistent with mitochondrial dysfunction pathway analysis, the oxidative phosphorylation pathway demonstrated increased levels of molecules involved in the electron transport chain of mitochondria.*

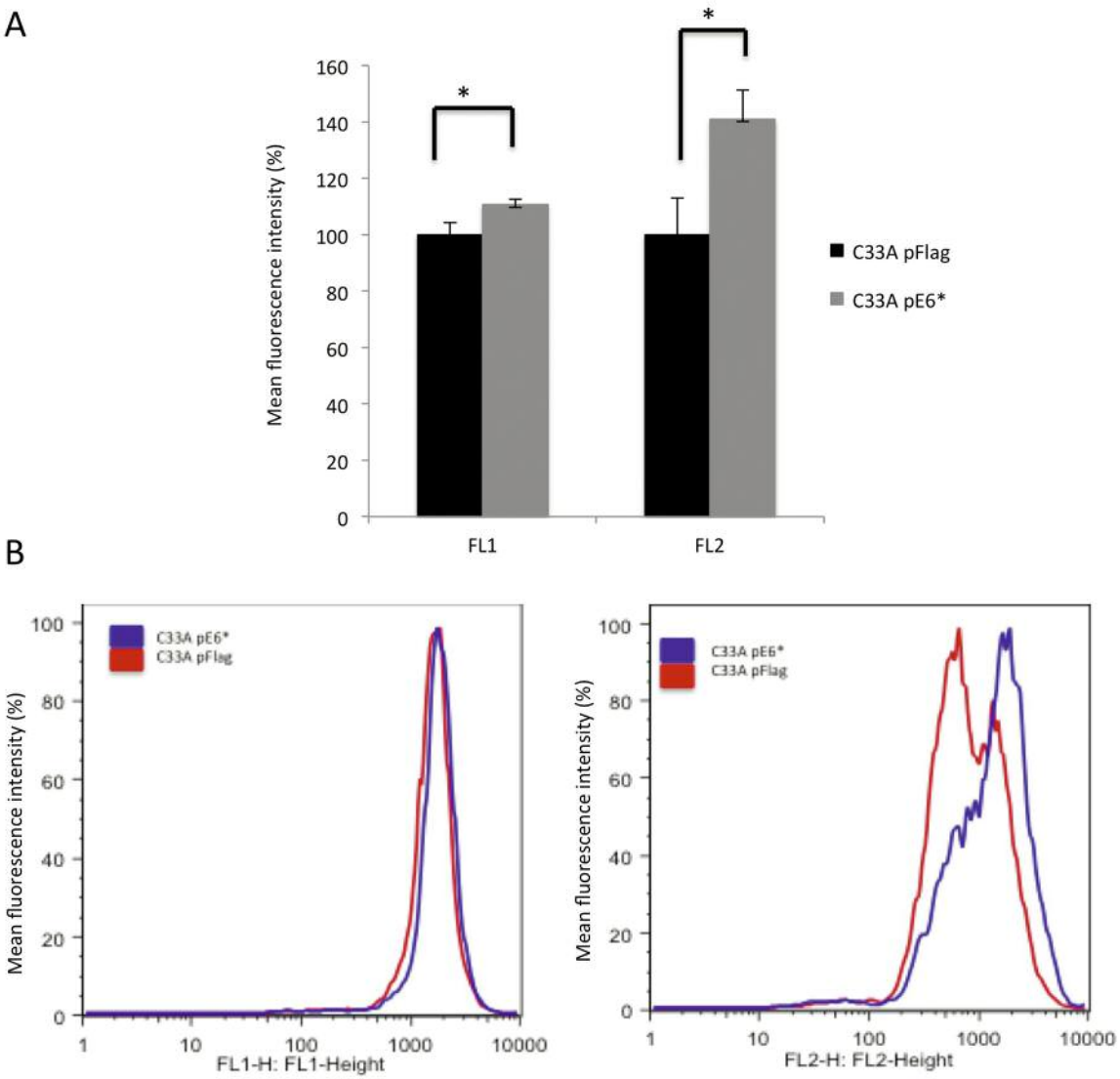

Figure 7. *Mitochondrial changes following E6* expression. Analysis of mitochondrial dysfunction by Mito ID assay and flow cytometry. Mito ID detects changes in mitochondrial activity. A: E6* caused greater depolarization of mitochondria in C33A pE6* cells compared to those in C33A pFlag cells. The FL2 channel, on the other hand, detected a substantial shift in orange fluorescence, inferring increased dye aggregation and suggesting that a large population of mitochondria in C33A pE6* cells were energized. Mean Fluorescence Intensity (MFI). B: Mitochondrial membrane depolarization in SiHa pE6* cells was augmented compared to SiHa pFlag cells, which is demonstrated by the detection of increased green fluorescence in the FL1 channel. The increased mitochondrial membrane depolarization in SiHa pE6* cells was accompanied by a decrease in energized mitochondria, as indicated by a decrease in the orange fluorescence signal detected by the FL2 channel. Triplicate measurements of the mean fluorescence intensity of carbocyanine were performed to generate the bar graph. The mean fluorescence intensity of C33A pFlag and SiHa pFlag cells was set at 100%. Error bars represent the standard deviations. *Significantly different at $p<0.05$. MFI: Mean fluorescence intensity.*

control cells, although C33A pE6* cells overall suffered more minimal to medium DNA injury than did the C33A pFlag cells.

Interestingly, SiHa and C33A pE6* cells, with more DNA damage compared to their controls, displayed significantly lower GSH levels (Figure 8C; $p<0.05$). Therefore, the findings presented herein further endorse the inverse relationship between cellular DNA damage and antioxidant capacity. Of note, GSH levels in C33A pE6* cells were the lowest of all four groups of cells. This observation is congruent with the fact that C33A pE6* cells are the most likely to display DNA damage (9B), although the extent of this DNA damage is less severe in these cells compared to the other three cell lines.

Discussion

Over the years, major discoveries in virology and oncology have allowed us to grasp the transformative impact of the E6 oncoprotein. Although a wealth of information exists regarding the roles of full-length HPV16 E6 in pathways involving apoptosis (30-34) and the mechanisms used by this virus to evade the immune system (35), much less is known of the activities of its splice variants that are present only in HR-HPVs, collectively known as E6*.

In this report, we analyzed the proteomes and cellular pathways of HPV^+ and HPV^- cervical carcinoma cells expressing HPV16 E6* to gain a better understanding of the anti-oncogenic mechanisms by which E6* reduces tumor formation, as previously reported (13). SiHa and C33A cells were selected as models to determine how E6* interacts with its cellular host in the presence and absence of other HPV proteins. Because these two cell lines are derived from very different patients with cervical carcinoma and differ in both HPV status and p53 level (C33A has mutant p53 and other structural abnormalities) (36), we expected to see variations in the changes to the cellular proteome observed following expression of E6*. Indeed, proteomic analysis revealed that E6* produces unique effects in different cellular environments. For example, the top canonical pathways affected by E6* in SiHa cells included the ILK pathway, whereas mitochondrial dysfunction and OXPHOS pathways were most affected in C33A cells (Tables I and II).

Proteomic analysis demonstrated that the β-integrin pathway *via* ILK was activated in SiHa cells (Table I, Figure 3A), but not in C33A cells that expressed E6* (Table II), and immunoblotting analysis suggested that the level of β1-integrin in SiHa cells was increased (Figure 3B). The integrin family, in general, mediates interactions between the extracellular matrix (ECM) and cells, as well as cell-to-cell communications. Kindlin-1, a co-stimulatory molecule of β1-integrin inside-out signaling (as well as a mediator for outside-in communication) (37), was also up-regulated (Figure 3C), and the increase in its expression is consistent with the amplification of β1-integrin expression. Kindlin-1 is known to regulate actin cytoskeleton remodeling during cell translocation, circumferential actin assembly and cell spreading *via* Rho GTPase signaling (19). Therefore, we probed further downstream of the β-integrin pathway and found that E6* expression in SiHa cells reduced RhoA GTPase expression, although this change was not as prominent in C33A pE6* cells (Figure 3D). Importantly, RhoA operates under the regulation of numerous molecules to execute cellular changes. Changes in RhoA expression mediated by kindlin-1 are reported to assist in actin cytoskeleton remodeling and the formation of stress fibers (19). Of note, RhoA is capable of integrating and transducing cell-shape and soluble growth-factor cues into regulatory signals that influence cell lineage (22), which may induce the expression of early differentiation markers (19). Interestingly, our data suggested that E6* may also slightly increase RhoA levels in C33A pE6* cells, although direct stimulation of RhoA by kindlin-1 in these cells was lacking (Figure 3C). This may reflect subtle, yet significant, differences in the upstream molecules controlling RhoA activity and subsequent cellular behavior. For example, it has been shown that changes in Rho activity mediated by kindlin are distinct from Rho activity mediated by G protein-coupled receptor or tumor necrosis factor (38-40). Such complexity may be necessary for ubiquitous, downstream molecules. Clearly, an E6*-mediated increase, *via* ILK, in ECM interactions and in cell–cell communication would have the potential to reduce tumor growth in SiHa cells.

The involvement of these particular proteins from the β-integrin signaling pathway in our system inferred that cell shape could be affected by the expression of E6*. Indeed, morphological analysis allowed the detection of a visible difference between SiHa pE6* cells, with reduced RhoA and increased β1-integrin expression, and SiHa pFlag cells (Figure 4A). These morphological observations are harmonious with previous research linking cell spreading and outward membrane protrusion to reduced RhoA activity and cell migration (27), and these observed differences might be attributed to changes in expression of β-integrin pathway components mediated by E6*.

The expression of E6* in SiHa cells may, indeed, affect cell differentiation factors by modifying the expression pattern of β-integrin signaling molecules. According to our proteomic data and supporting experiments, ALPP levels and activity were significantly reduced in SiHa pE6* cells due to the increased expression of E6* (Figure 5). ALPP is a ubiquitous membrane-bound enzyme and is categorized into a family of four isoenzymes, each with different functions and biochemical properties. Some ALPPs can be found in normal, as well as cancerous tissues (23). High ALPP is correlated with pluripotency and undifferentiated cell phenotypes, whereas low ALPP activity implies differentiation (23). Moreover, ALPP is currently most recognized and valued as a prognostic factor in cancer (such as ovarian and colorectal carcinomas) (24, 25), with a decrease in ALPP being defined as a positive indicator of patient survival. A reduction in ALPP activity is reported to accompany overexpression of the tumor suppressor protein phosphatase 2 (PP2A) (41). Although our investigation did not include validation of an E6*-mediated increase in PP2A, a previous study reported the co-localization of β1-integrin and PP2A (42). Furthermore, one investigation reported that the up-regulation of colonic ALPP in response to inflammation might serve as a protective mechanism against oxidative stress (43), implying that the down-regulation of

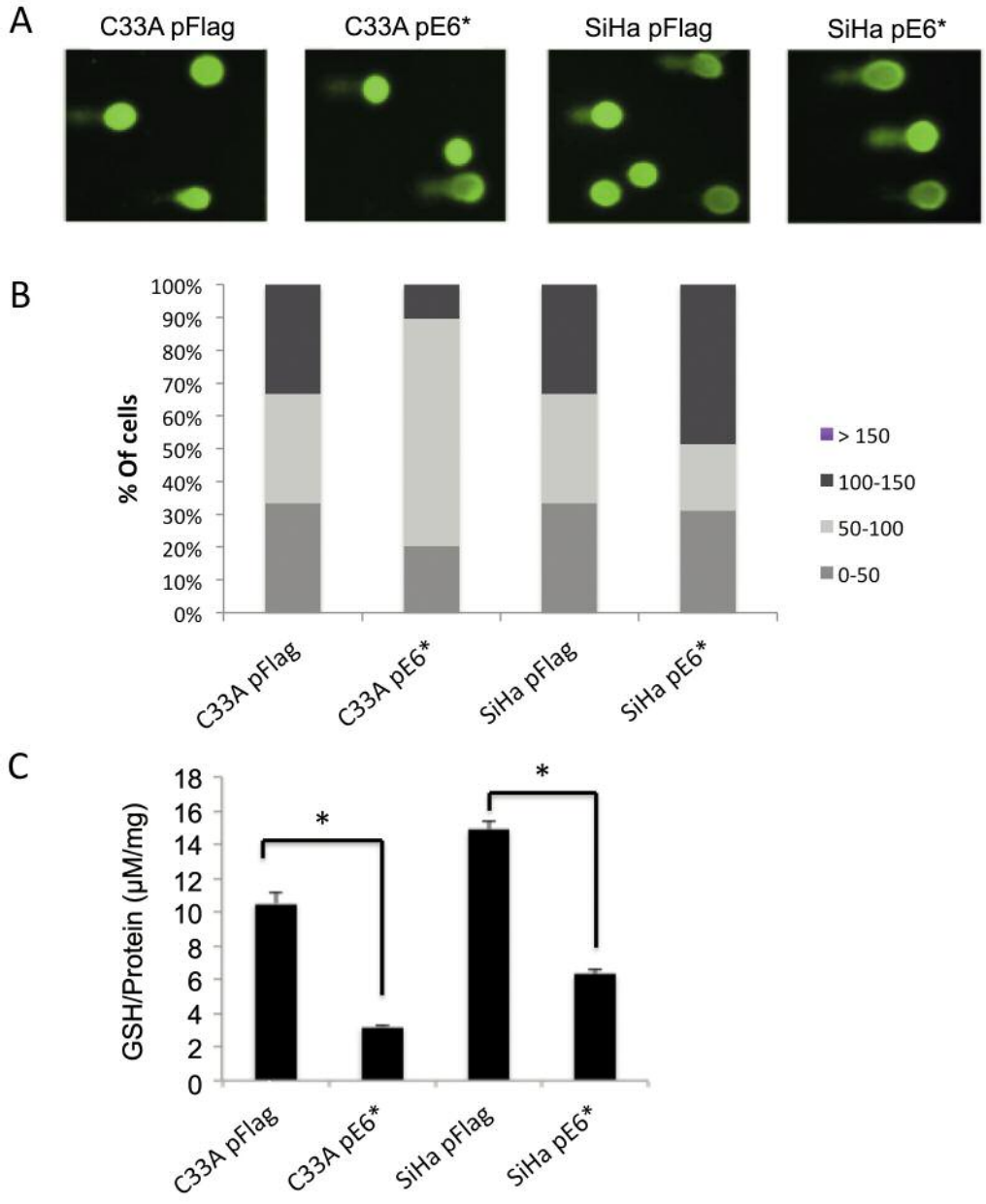

Figure 8. *E6*-mediated changes in DNA damage and glutathione (GSH) levels. A: Measurement of DNA damage in SiHa and C33A cells by the comet assay. Representative images from comet assay showing variations in tail length between E6*-expressing cells and control cells. SiHa pE6* cells displayed the most severe DNA damage of all the groups. B: Percentage of cells with different degrees of DNA damage. SiHa pE6* and C33A pE6* cells exhibited comparable levels of DNA damage overall. However, a greater percentage of SiHa pE6* cells had more severe DNA damage than did SiHa pFlag, C33A pFlag, and C33A pE6* cells. C33A pE6* cells suffered more DNA injury compared to C33A pFlag cells, although the distribution of the extent of DNA damage was different. C: Measurement of GSH level in SiHa and C33A cells by GSH-Glo assay. Although SiHa pFlag cells displayed more glutathione than C33A pFlag cells, E6* appeared to reduce the amount of GSH in both SiHa and C33A cells proportional to their initial levels of GSH. Triplicate measurements of GSH concentration were performed to generate the graph, and error bars represent the standard deviations. *Significantly different at $p<0.05$.*

ALPP might render cells more susceptible to insult. Together, these observations, as well as those studies classifying certain forms of ALPP as stem cell markers and a target of developmental and differentiation processes (23, 41), make it a fascinating subject of study in the context of cancer research. Therefore, the investigation of their expression in diverse conditions could prove important, and this study may assist in such efforts.

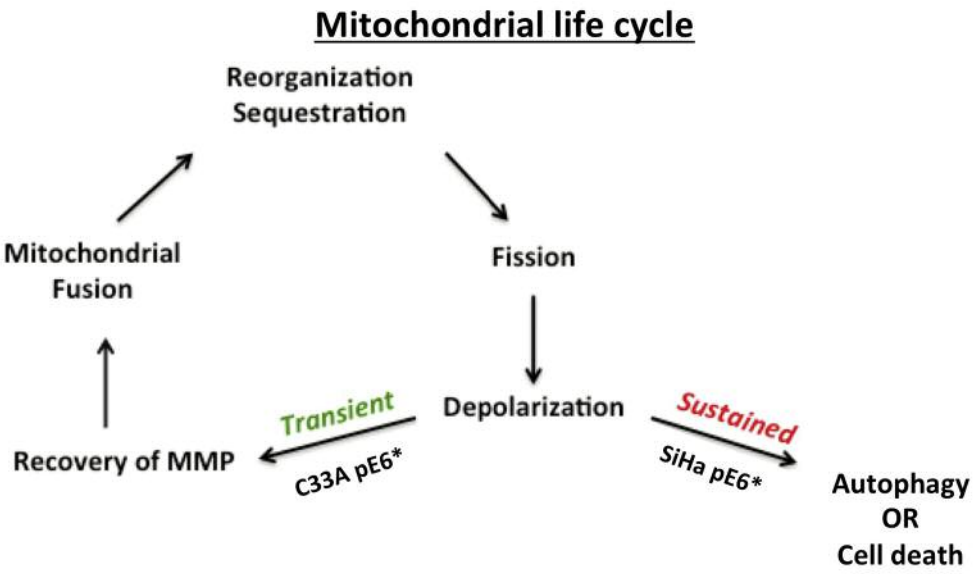

Figure 9. *The mitochondrial life cycle. This schematic of the mitochondrial life cycle was adapted from Hyde and Twig et al. (30). E6*-mediated changes in mitochondrial function may be cell-specific and may activate different mechanisms affecting cell survival and cell death in SiHa and C33A cells. Mitochondrial dynamics are highly complex and determine the condition and fate of mitochondria within a cell. Mitochondria in the same cell can be at different stages of the mitochondrial life cycle. Among the multiple states mitochondria can assume, mitochondrial membrane depolarization is key and may be reversible. MMP: Mitohondrial membrane polarization.*

The mitochondrial dysfunction and OXPHOS pathways are closely related and are profoundly affected by the overexpression of E6*, particularly in C33A cells (Figure 6A and B). The study of both pathways led to the conclusion that electron transport chain complex molecules are highly activated in *E6**-expressing C33A cells compared to control C33A cells. Our data showed that mitochondria in C33A pE6* cells experienced more depolarization, and were more energized compared to those in C33A pFlag cells (Figure 7A). It is possible that the up-regulation of electron transport chain molecules, as seen in C33A pE6* cells, could reflect the mitochondria's attempt to adapt to the stresses imposed by E6*-mediated increases in ROS production (17). Some researchers speculate that certain conditions in the mitochondria (such as alkalization) can cause transient depolarization, which is repetitive and reversible (44), leading to suppression of ROS generation (45). In fact, protective mechanisms engaging the mitochondria have been described in other types of epithelial-derived cancer (46).

We were somewhat surprised to find that mitochondrial injury was greatest in SiHa pE6* cells, as determined by Mito ID analysis (Figure 7B), since significant changes in the associated protein levels were not detected by our proteomic data when SiHa pE6* cells were compared to SiHa controls. It is possible that the expression of *E6** might stress SiHa cells enough, through increased ROS (17), to cause harm to mitochondria that is beyond repair. Therefore, it is reasonable to suppose that such cells, experiencing oxidative stress and continued ROS production, could undergo sustained MMP (44), rather than less-damaging transient depolarization. Therefore, these two mitochondrial mechanisms might contribute to the different effects *E6** has on MMP in SiHa and C33A cells.

The mechanisms regulating MMP fluctuations in mitochondria have not been fully elucidated because the dynamics controlling the depolarized and energized states are highly complex. According to the mitochondrial life-cycle model summarized in Figure 9 [see (47, 48)], our data may suggest that mitochondria in C33A pE6* experience transient, reversible depolarization, resulting in a larger population of re-energized mitochondria, whereas those in SiHa pE6* cells may suffer more harm by sustained depolarization.

The differences detected in mitochondrial depolarization between the SiHa and C33A cell lines may help explain cell type-specific vulnerabilities to E6*-mediated increases in oxidative stress. Our studies suggest that understanding the role of mitochondrial dysfunction in cancer is essential to the study of cancer cell behavior and possibly overcoming therapy resistance (49).

Boland *et al.* describe several types of mitochondrial dysfunction that can occur in response to cell stress: i) loss of MMP leading to membrane depolarization, ii) opening of mitochondrial membrane pores causing mitochondrial membrane permeability; iii) altered expression of molecules

in the ETC (27), resulting in defective respiration and oxygen consumption; iv) an imbalance in the expression of mitochondrial *versus* nuclear proteins, leading to initiation of the unfolded mitochondrial protein response; v) oxidative damage of the mitochondrial genome; and vi) inappropriate release of cytochrome *c*, causing pre-mature apoptosis (49). Our proteomic studies, and the subsequent experiments performed to validate those results, detected the first three out of these six mechanisms of mitochondrial dysfunction, although many of them overlap. For example, defective respiration might be associated with mitochondrial membrane depolarization, since the proton gradient is coupled to the redox reactions occurring along the ETC and is dependent on the MMP. This premise is further illustrated by our own data, that show involvement of both the OXPHOS and mitochondrial dysfunction pathways in C33A cells under the stresses of *E6** expression.

While our study did not test the possibility that oxidative stress caused by E6* induces mitochondrial DNA damage (see mechanism v above), our data do show that *E6** overexpression increases nuclear DNA damage in both SiHa and C33A cells, with the damage more severe in SiHa E6* cells (Figure 9A and B). Intriguingly, nuclear DNA damage has been linked to mitochondrial dysfunction in chronic disease (50). Thus, we could speculate that the mitochondrial dysfunction detected by Mito ID in SiHa pE6* cells (Figure 7B) may correspond to the increased severity of DNA damage.

Because the cell is dependent on antioxidants for protection from oxidative stress, GSH is essential for cell survival. Not surprisingly, GSH levels were affected by *E6** expression in both SiHa and C33A cells (Figure 9C), as cellular oxidative stress is well known to deplete the GSH level. However, researchers are now realizing that a reduced GSH level may also be an early marker of cell death and essential to apoptosis (51). The same reports also state that GSH is accompanied by cytochrome *c* release, suggesting the presence of a more permeable mitochondrial membrane. Furthermore, studies reveal that GSH interacts with the cytoskeleton through glutathionylation, causing changes in organization and function (52, 53). However, more research is required to investigate whether E6* facilitates interactions between antioxidant and cytoskeleton components. In any case, the reduction in GSH seen following *E6** overexpression in both SiHa and C33A cells has the potential to predispose the expressing cells to DNA damage and to apoptosis, thereby potentially contributing to reduced tumor growth.

Additionally, it might be the fact that the increased level of DNA damage in C33A pE6* cells, in particular, reaches a degree of chronic oxidative stress that depletes GSH stores to a greater extent (54). Because the GSH level in C33A cells is lower than that in SiHa cells this observation may highlight the influence and efficacy of additional intact compensatory antioxidative stress mechanisms in C33A cells other than those involving GSH (55). These mechanisms may be more intrinsically linked to mitochondria, as discussed earlier, evoking mitohormetic responses (56).

Overall, our pathway analysis suggests that the mechanisms by which E6* reduces tumor growth in SiHa cells may include an increase in the activation of β1-integrin-mediated pathways, thereby increasing ECM and cell–cell communication; reduction of ALPP expression, thus enhancing differentiation and sensitivity of expressing cells to insults; changes in mitochondrial function and an increase in more severe DNA damage, thereby compromising cell viability; and a decrease in the protective molecule, GSH. E6* may reduce tumor growth in C33A cells by increasing the amount of moderate DNA damage, consequently forfeiting cell viability (but to a lesser extent than the impact of DNA damage to SiHa cells). Overexpression of E6* in C33A cells also reduces the level of GSH, which might activate other protective responses not triggered in SiHa cells, and involve mitochondrial dysfunction pathways. Differences in the cellular response to E6*, as exemplified here, may also help explain why SiHa pE6* tumors exhibited a greater growth reduction than did C33A pE6* tumors, as previously reported (13). This investigation has, therefore, added to our knowledge of the cellular pathways through which HPV16 E6* influences cell behavior, while suggesting possible avenues for explanation into novel and effective therapeutic options.

Conclusion

Among virus-associated malignancies, HPV-mediated cervical cancer represents one of the best-defined models of virus-mediated carcinogenesis. As such, the data presented here reveal novel E6*-mediated changes to the cellular proteome in HPV^+ and HPV^- milieus, allowing us to compare and contrast the biological effects of *E6** in different cancer settings. We report that the overexpression of *E6** is capable of influencing components of the β-integrin and mitochondrial dysfunction signaling pathways in SiHa and C33A cells, respectively. This investigation has added to our knowledge of the cellular pathways through which HPV16 E6* affects cell behavior. Furthermore, the insights conveyed in this study could lead to new and exciting directions for the role of E6* in cancer research.

Conflicts of Interest

The Authors have no competing financial interests in relation to the work described.

Acknowledgements

The Authors would like to thank Loma Linda University Mass Spectrometry Facility for technical support in proteome analysis. This work was supported in part by NCI grant RO1 CA095461 from the National Institutes of Health.

References

1 WHO 2013 Sexual and Reproductive Health 2013. Available from: http://www.who.int/reproductivehealth/topics/cancers/en/.

2 Hoste G, Vossaert K and Poppe WA: The clinical role of HPV testing in primary and secondary cervical cancer screening. Obstet Gynecol Int *2013*: 610373, 2013.

3 Parkin DM and Bray F: Chapter 2: The burden of HPV-related cancers. Vaccine *24(Suppl 3)*: S3/11-25, 2006.

4 Jung YS, Kato I and Kim HR: A novel function of HPV16-E6/E7 in epithelial-mesenchymal transition. Biochem Biophys Res Commun *435(3)*: 339-344, 2013.

5 Williams VM, Filippova M, Soto U and Duerksen-Hughes PJ: HPV-DNA integration and carcinogenesis: Putative roles for inflammation and oxidative stress. Future Virol *6(1)*: 45-57, 2011.

6 Scott B and Van de Pol AJK: Papillomavirus E6 oncoproteins. Virology *445*: 115-137, 2013.

7 Niccoli S, Abraham S, Richard C and Zehbe I: The Asian-American E6 variant protein of human papillomavirus 16 alone is sufficient to promote immortalization, transformation, and migration of primary human foreskin keratinocytes. J Virol *86(22)*: 12384-12396, 2012.

8 Tungteakkhun SS and Duerksen-Hughes PJ: Cellular binding partners of the human papillomavirus E6 protein. Arch Virol *153(3)*: 397-408, 2008.

9 Rosenberger S, De-Castro Arce J, Langbein L, Steenbergen RD and Rosl F: Alternative splicing of human papillomavirus type-16 E6/E6* early mRNA is coupled to EGF signaling *via* ERK1/2 activation. Proc Natl Acad Sci USA *107(15)*: 7006-7011, 2010.

10 Chakrabarti O, Veeraraghavalu K, Tergaonkar V, Liu Y, Androphy EJ, Stanley MA and Krishna S: Human papillo-mavirus type 16 E6 amino acid 83 variants enhance E6-mediated MAPK signaling and differentially regulate tumorigenesis by notch signaling and oncogenic ras. J Virol *78(11)*: 5934-5945, 2004.

11 Pim D, Tomaic V and Banks L: The human papillomavirus (HPV) E6* proteins from high-risk, mucosal HPVs can direct degradation of cellular proteins in the absence of full-length E6 protein. J Virol *83(19)*: 9863-9874, 2009.

12 Filippova M, Johnson MM, Bautista M, Filippov V, Fodor N, Tungteakkhun SS, Williams K and Duerksen-Hughes PJ: The large and small isoforms of human papillomavirus type 16 E6 bind to and differentially affect procaspase 8 stability and activity. J Virol *81(8)*: 4116-4129, 2007.

13 Filippova M, Evans W, Aragon R, Filippov V, Williams VM, Hong L, Reeves ME and Duerksen-Hughes P: The small splice variant of HPV16 E6, E6, reduces tumor formation in cervical carcinoma xenografts. Virology *450-451*: 153-164, 2014.

14 Hernandez-Lopez HR and Graham SV: Alternative splicing in human tumour viruses: A therapeutic target? Biochem J *445(2)*: 145-156, 2012.

15 Schneider CA, Rasband WS and Eliceiri KW: NIH image to ImageJ: 25 years of image analysis. Nat Methods *9(7)*: 671-675, 2012.

16 Filippova M, Filippov V, Williams VM, Zhang K, Kokoza A, Bashkirova S and Duerksen-Hughes P: Cellular levels of oxidative stress affect the response of cervical cancer cells to chemotherapeutic agents. Biomed Res Int *2014*: 574659, 2014.

17 Williams VM, Filippova M, Filippov V, Payne KJ and Duerksen-Hughes P: Human papillomavirus type 16 E6* induces oxidative stress and DNA damage. J Virol *88(12)*: 6751-6761, 2014.

18 Wu C and Dedhar S: Integrin-linked kinase (ILK) and its interactors: A new paradigm for the coupling of extracellular matrix to actin cytoskeleton and signaling complexes. J Cell Biol *155(4)*: 505-510, 2001.

19 Has C, Herz C, Zimina E, Qu HY, He Y, Zhang ZG, Wen TT, Gache Y, Aumailley M and Bruckner-Tuderman L: Kindlin-1 is required for RHOGTPase-mediated lamellipodia formation in keratinocytes. Am J Pathol *175(4)*: 1442-1452, 2009.

20 Tkach V, Bock E and Berezin V: The role of RHOA in the regulation of cell morphology and motility. Cell Motil Cytoskeleton *61(1)*: 21-33, 2005.

21 Leung T, Chen XQ, Manser E and Lim L: The p160 RHOA-binding kinase ROK alpha is a member of a kinase family and is involved in the reorganization of the cytoskeleton. Mol Cell Biol *16(10)*: 5313-5327, 1996.

22 McBeath R, Pirone DM, Nelson CM, Bhadriraju K and Chen CS: Cell shape, cytoskeletal tension, and rhoa regulate stem cell lineage commitment. Dev Cell *6(4)*: 483-495, 2004.

23 Stefkova K, Prochazkova J and Pachernik J: Alkaline phosphatase in stem cells. Stem Cells Int *2015*: 628368, 2015.

24 Ben-Arie A, Hagay Z, Ben-Hur H, Open M and Dgani R: Elevated serum alkaline phosphatase may enable early diagnosis of ovarian cancer. Eur J Obstet Gynecol Reprod Biol *86(1)*: 69-71, 1999.

25 Saif MW, Alexander D and Wicox CM: Serum alkaline phosphatase level as a prognostic tool in colorectal cancer: A study of 105 patients. J Appl Res *5(1)*: 88-95, 2005.

26 Hai-Yong Ren L-LS, Heng-Yuan Li, and Zhao-Ming Ye: Prognostic significance of serum alkaline phosphatase level in osteosarcoma: A meta-analysis of published data. BioMed Research International *2015*: 11, 2015.

27 Arthur WT, Petch LA and Burridge K: Integrin engagement suppresses RHOA activity *via* a c-SRC-dependent mechanism. Curr Biol *10(12)*: 719-722, 2000.

28 Joshi DC and Bakowska JC: Determination of mitochondrial membrane potential and reactive oxygen species in live rat cortical neurons. J Vis Exp *51*: e2704, 2011.

29 Cui H, Kong Y and Zhang H: Oxidative stress, mitochondrial dysfunction, and aging. J Signal Transduct 2012: 646354, 2012.

30 Garnett TO and Duerksen-Hughes PJ: Modulation of apoptosis by human papillomavirus (HPV) oncoproteins. Arch Virol *151(12)*: 2321-2335, 2006.

31 Garnett TO, Filippova M and Duerksen-Hughes PJ: Accelerated degradation of FADD and procaspase 8 in cells expressing human papilloma virus 16 E6 impairs TRAIL-mediated apoptosis. Cell Death Differ *13(11)*: 1915-1926, 2006.

32 Filippova M, Parkhurst L and Duerksen-Hughes PJ: The human papillomavirus 16 E6 protein binds to FAS-associated death domain and protects cells from FAS-triggered apoptosis. J Biol Chem *279(24)*: 25729-25744, 2004.

33 Filippova M, Brown-Bryan TA, Casiano CA and Duerksen-Hughes PJ: The human papillomavirus 16 E6 protein can either protect or further sensitize cells to TNF: Effect of dose. Cell Death Differ *12(12)*: 1622-1635, 2005.

34 Yuan CH, Filippova M and Duerksen-Hughes P: Modulation of apoptotic pathways by human papillomaviruses (HPV): Mechanisms and implications for therapy. Viruses *4(12)*: 3831-3850, 2012.

35 Ganguly N and Parihar SP: Human papillomavirus E6 and E7 oncoproteins as risk factors for tumorigenesis. J Biosci *34(1)*: 113-123, 2009.

36 Zimonjic DB, Simpson S, Popescu NC and DiPaolo JA: Molecular cytogenetics of human papillomavirus-negative cervical carcinoma cell lines. Cancer Genet Cytogenet *82(1)*: 1-8, 1995.
37 Meves A, Stremmel C, Gottschalk K and Fassler R: The kindlin protein family: New members to the club of focal adhesion proteins. Trends Cell Biol *19(10)*: 504-513, 2009.
38 Shen B, Delaney MK and Du X: Inside-out, outside-in, and inside-outside-in: G protein signaling in integrin-mediated cell adhesion, spreading, and retraction. Curr Opin Cell Biol *24(5)*: 600-606, 2012.
39 Meiri D, Marshall CB, Mokady D, LaRose J, Mullin M, Gingras AC, Ikura M and Rottapel R: Mechanistic insight into GPCR-mediated activation of the microtubule-associated RHOA exchange factor gEF-H1. Nat Commun *5*: 4857, 2014.
40 Kant S, Swat W, Zhang S, Zhang ZY, Neel BG, Flavell RA and Davis RJ: TNF-stimulated MAP kinase activation mediated by a rho family GTPase signaling pathway. Genes Dev *25(19)*: 2069-2078, 2011.
41 Okamura H, Yoshida K, Yang D and Haneji T: Protein phosphatase 2A Calpha regulates osteoblast differentiation and the expressions of bone sialoprotein and osteocalcin *via* osterix transcription factor. J Cell Physiol *228(5)*: 1031-1037, 2013.
42 Ivaska J, Nissinen L, Immonen N, Eriksson JE, Kahari VM and Heino J: Integrin alpha 2 beta 1 promotes activation of protein phosphatase 2a and dephosphorylation of AKT and glycogen synthase kinase 3 beta. Mol Cell Biol *22(5)*: 1352-1359, 2002.
43 Lalles JP: Intestinal alkaline phosphatase: Novel functions and protective effects. Nutr Rev *72(2)*: 82-94, 2014.
44 Swanson RA: Neuroglia. Ransom HKaB (ed.). pp. 425, 1996.
45 Hattori T, Watanabe K, Uechi Y, Yoshioka H and Ohta Y: Repetitive transient depolarizations of the inner mitochondrial membrane induced by proton pumping. Biophys J *88(3)*: 2340-2349, 2005.
46 Whitaker-Menezes D, Martinez-Outschoorn UE, Flomenberg N, Birbe RC, Witkiewicz AK, Howell A, Pavlides S, Tsirigos A, Ertel A, Pestell RG, Broda P, Minetti C, Lisanti MP and Sotgia F: Hyperactivation of oxidative mitochondrial metabolism in epithelial cancer cells in situ: Visualizing the therapeutic effects of metformin in tumor tissue. Cell Cycle *10(23)*: 4047-4064, 2011.
47 Twig G and Shirihai OS: The interplay between mitochondrial dynamics and mitophagy. Antioxid Redox Signal *14(10)*: 1939-1951, 2011.
48 Hyde BB, Twig G and Shirihai OS: Organellar *vs*. cellular control of mitochondrial dynamics. Semin Cell Dev Biol *21(6)*: 575-581, 2010.
49 Boland ML, Chourasia AH and Macleod KF: Mitochondrial dysfunction in cancer. Front Oncol *3*: 292, 2013.
50 Mercer JR, Cheng KK, Figg N, Gorenne I, Mahmoudi M, Griffin J, Vidal-Puig A, Logan A, Murphy MP and Bennett M: DNA damage links mitochondrial dysfunction to atherosclerosis and the metabolic syndrome. Circ Res *107(8)*: 1021-1031, 2010.
51 Franco R and Cidlowski JA: Apoptosis and glutathione: Beyond an antioxidant. Cell Death Differ *16(10)*: 1303-1314, 2009.
52 Carletti B, Passarelli C, Sparaco M, Tozzi G, Pastore A, Bertini E and Piemonte F: Effect of protein glutathionylation on neuronal cytoskeleton: A potential link to neurodegeneration. Neuroscience *192*: 285-294, 2011.
53 John Gardiner RO and Jan Marc: The nervous system cytoskeleton under oxidative stress. Diseases *1*: 15, 2013.
54 Hashimoto K, Takasaki W, Yamoto T, Manabe S, Sato I and Tsuda S: Effect of glutathione (GSH) depletion on DNA damage and blood chemistry in aged and young rats. J Toxicol Sci *33(4)*: 421-429, 2008.
55 Birben E, Sahiner UM, Sackesen C, Erzurum S and Kalayci O: Oxidative stress and antioxidant defense. World Allergy Organ J *5(1)*: 9-19, 2012.
56 Yun J and Finkel T: Mitohormesis. Cell Metab *19(5)*: 757-766, 2014.

Received January 12, 2016
Revised March 30, 2016
Accepted March 31, 2016